

SEISMIC BEHAVIOR OF R/C NON-STRUCTURAL WALLS

T. Hitaka¹ and Y. Imadzu²

¹ Associate Prof., Disaster Prevention Research Institute, Kyoto University, Kyoto, Japan

² Engineer, Taisei Co., Tokyo, Japan
Email: toko.h@ay2.ecs.kyoto-u.ac.jp

ABSTRACT :

Typically, in apartment houses, there are large openings in the walls facing a balcony or corridor. In small apartment houses, the structural contribution of these walls to the building's seismic response is negligible because these walls are quite small. However, in large apartment buildings, which have relatively large walls, the effect the walls to the building's seismic behavior can be substantial. Loading tests were conducted on three steel frame – RC wall specimens to investigate the structural behavior of these walls, and to create numerical models useful for frame analyses based on the test results presented in this paper and other reference.

KEYWORDS: reinforced concrete, non-structural wall, loading test, numerical model

1. INTRODUCTION

Shown in Fig. 1a is a record of damages observed in a 14 story condominium of steel reinforced concrete (SRC), called simply as KT hereafter (AIJ, 2005). KT, completed in 1998, was designed as a pure moment frame. A dynamic analysis using a 2D frame model, based on its design document and a ground motion recorded at a site near KT's location, gives the building's maximum response as represented with a filled circle in Fig. 1b; drifts are large but distributed fairly evenly along height of the building. Actually, as found in the post-quake survey of the building, non-structural walls, which have 150mm thickness and are made of reinforced concrete (RC), had sustained substantial damages, mostly in the lower stories. The residual deformation in the steel door frames also showed that drift was larger in lower stories. These observations appear to suggest that the non-structural walls had some effect on dynamic response of the building.

KT has two types of wall configuration as schematically shown in Fig. 1c. One is a wall connected to beams but detached from columns by doors and/or windows, called B-B walls, hereafter. The other is a wall in which a B-B wall connects to a wall segment filling lower portion of a window; this wall segment is called C-B wall in the following. Effects of the C-B walls on seismic performance of frames were investigated after Off-Miyagi Earthquake in 1978, where brittle shear failure of RC columns attributed to C-B walls was reported (AIJ, 2005). Since 1997 in Japan, C-B walls and B-B walls alike should be designed such that there will be only small (ideally, zero) force transfer between these walls and frame. This design goal is usually achieved by making a gap, or a so-called "structural slit," between a wall and a frame.

Unfortunately, these slits are sometimes constructed insufficiently, and KT turned out to be one such case. KT was a SRC structure, a structure type known to have a good shear performance. Therefore, unlike RC columns, brittle shear failure of columns would not have occurred in this building even with such deficient slits. However, the stiffness and story shear capacities "unexpectedly" added by RC non-structural walls with inadequate slitting may cause concentration of deformation. As mentioned earlier, due to the response of the RC walls, the drift in KT apparently concentrated in lower stories, in contrast to a fairly well distributed drifts predicted by the 2D dynamic analysis. Actually, this phenomenon can be explained using models that simulate behavior of these walls, as illustrated by the blank circles in Fig. 1b. Objective of the research in this paper is to create these models of B-B and C-B walls for frame analyses to evaluate performance of buildings with these walls. The models are created based on findings in the tests on RC B-B walls and C-B walls conducted by the authors, as well as those by other researchers (Ohkubo, et al., 1987; Sugiyama, et al., 2002).

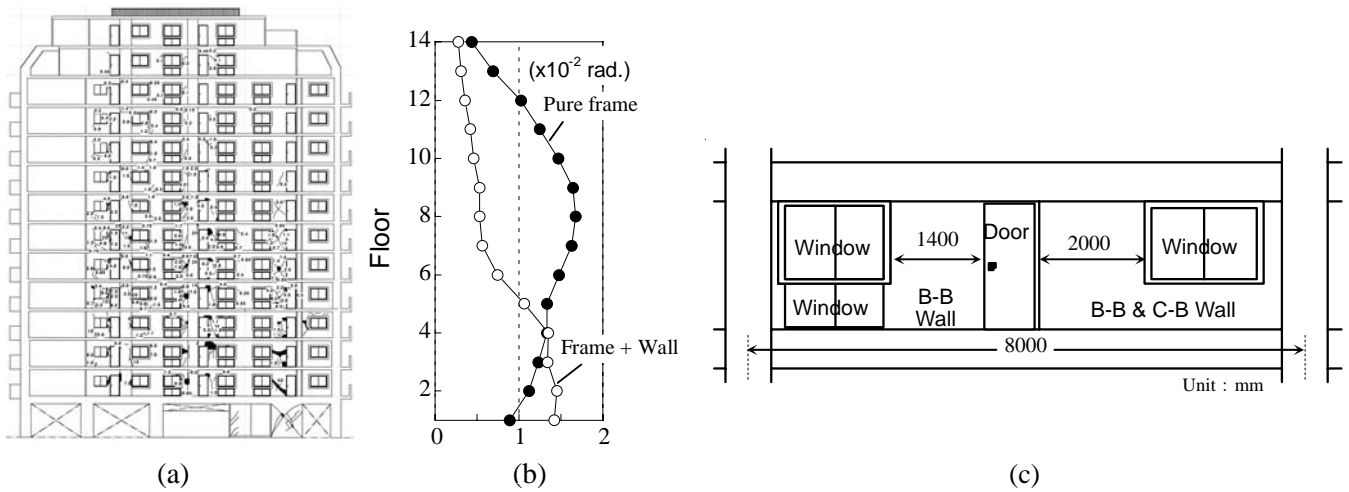


Fig. 1 RC non-structural walls of a condominium damaged in the 2005 West off Fukuoka Earthquake: (a) observed cracks; (b) estimated maximum story drift distribution; (c) configuration of typical non-structural walls.

2. TEST

2.1 Specimen

Tests were conducted on four specimens of approximately 1/2 scale, listed in Table 1. These are steel frames with RC walls and one pure steel frame specimen (LF) which was included to identify the steel frame's structural properties. The RC walls were designed based on the configuration and details of the walls of KT: the RC walls of KT are 150 mm thick and reinforced by deformed bars (D13@150, reinforcement ratio = 0.56%). Test parameters include configuration of walls and beam sections. The wall configuration is one of the following two types: a simple B-B wall and a combined type of wall where lower half of a B-B wall is connected to a C-B wall. In the tests, the former type of wall is reproduced in a M series specimen, and the latter, in MS series specimens. The walls of the specimens were 70 mm thick RC walls reinforced by D6@75 (reinforcement ratio = 0.60%), as shown in Fig. 2. The B-B wall is 800 mm wide and located in the middle of 2200 mm beam span. Height of the C-B walls was designated as 500 mm for a story height of 1250mm. The measured yield strength of the steel bars, concrete's compressive strength and Young's modulus were 333N/mm², 33 N/mm², and 32,000N/mm², respectively; Table 2 shows other material properties.

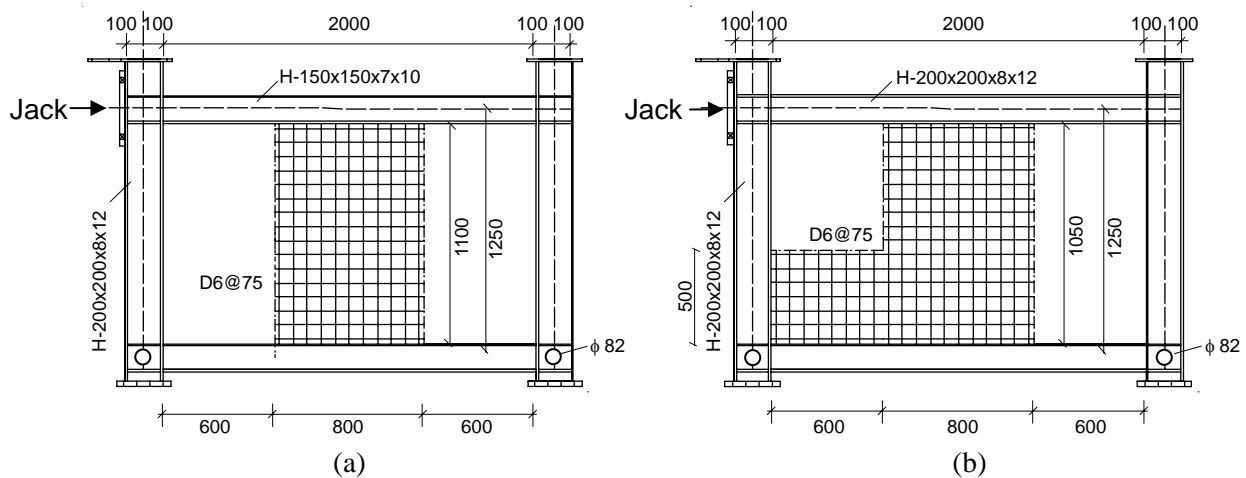


Fig. 2 Specimens: (a) LF-M; (b) HF-MS.

Steel was used for the frames in order for an accurate measurement of forces transferred between the wall and the frame. Therefore, in the specimens, the steel bars were connected to the frame through 3.2 mm thick, 16 mm wide fish plates welded to the steel members. In contrast, in KT, the end portion of steel bars was embedded in the SRC beams and columns. Before the tests, it was anticipated that this variation of frames of KT and the specimens might alter fixity of wall end boundaries, namely degree of anchorage of the reinforcing bars in the walls. However, we did not find significant effect of this difference in comparing our test results with those by other researchers, in which steel bars of the walls were embedded into the RC beams and columns.

Table 1 Specimens

Specimen	(1) Beam	(2) Wall	(3) [kN]	(4) [kN]	(5) [kN/mm]	(6) [kN]	(7) [kN]	(8) [kN/mm]
LF	H-150x150	-	332	-	18	242	-	18
LF-M	H-150x150	Mid-wall	386	202	86	390	196	72
LF-MS	H-150x150	Mid & Base	414	196	112	430	196	85
HF-MS	H-200x200	Mid & Base	556	206	168	556	192	151

(1) beam section; (2) configuration of RC wall; (3) measured maximum strength of specimens; (4) measured maximum strength of B-B walls; (5) measured stiffness; (6) – (8) analytically obtained maximum strength of specimens and B-B walls and stiffness.

Table 2 Material properties

Coupon		(1)	(2)	(3)
H-150x150x7x10	Flange	322	443	36
	Web	342	463	33
H-200x200x8x12	Flange	312	454	38
	Web	335	437	31

(1) yield strength (N/mm²); (2) ultimate strength (N/mm²); (3) elongation (x10⁻²).

2.2 Loading and Measurement

Fig. 3 shows the loading system. In each test, a vertical force (2% and 20% of the compressive strength of the steel columns for LF and HF series specimens, respectively) was applied by the vertical jack first. Then, steel rods were placed close to the side ends of the B-B walls with negligibly small initial tension; these rods will restrain separation between the wall and the beam, which would occur as the rods restrain rotation of the B-B walls. Lastly, horizontal load was applied, which was controlled by the drift angle (θ), defined as the displacements measured through transducers 1 and 3 in Fig. 4 divided by the frame height (h_f in Fig. 4). The specimens were pushed (defined as positive loading), then pulled (negative) through a pin installed close to the beam-column connection on the left side. The drift angle was increased by 0.25% after completing one cycle of loading until 2.0% of story drift angle was achieved. The loads applied through the hydraulic jacks were measured through load cells attached to the jacks. Story drifts and vertical and other displacements were measured through displacement transducers. Increments of the diagonal length of the RC wall segments (d_1 and d_2 in Fig. 4) were measured also through displacement transducers. These values were used to obtain shear distortion angle of the panels (γ) using the following equation,

$$\gamma = \frac{d_2 - d_1}{2h \cos \theta} \quad (2.1)$$

where geometric notations, d_1 , d_2 , h , θ are defined in Fig. 4. In MS series specimens, shear deformation may concentrate in the B-B wall (the upper part of the wall in Fig. 4). Thus, γ was obtained for each of three separate portions of the wall, as indicated in Fig. 4.

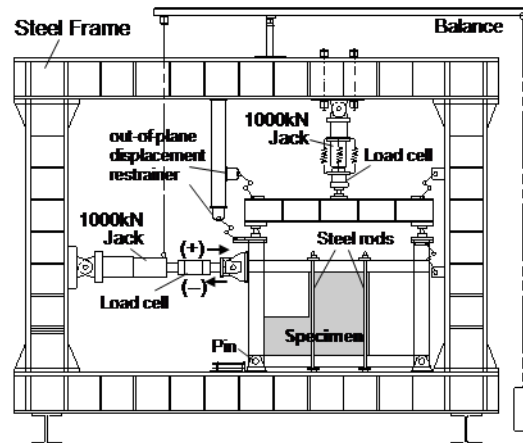


Fig. 3 Loading system.

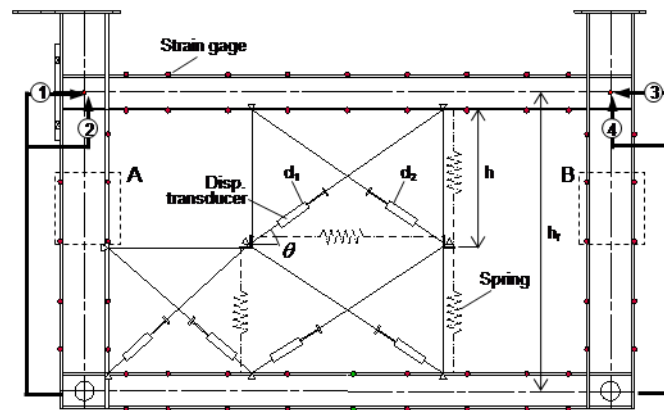


Fig. 4 Measurements.

Strain data were measured through strain gages installed on the steel frame. Especially, the strain data from the portions A and B in Fig. 4, where the steel will remain elastic to large deformation levels, were used to obtain bending moment induced in the sections, i.e. using the strain data from these portions of the columns and the Bernoulli-Euler hypothesis, the curvature of these sections were calculated. The shear response of the columns (Q_f) were then calculated using the moment of inertia and Young's modulus of the steel members, 2.05×10^5 N/mm². The shear force carried by the B-B wall, Q_w , was obtained by subtracting Q_f from H_t . It was confirmed that the difference between Q_f and the horizontal force measured by the load cell (H_t) was smaller than 5% for specimen LF. Also, two strain gages were mounted on each steel rod to measure induced tensile forces.

3. TEST RESULTS

3.1 Overall behavior

The hysteresis loops of the specimens and B-B walls are shown in Fig. 5a. Note that for the B-B wall of Specimen HF-MS, only the loops obtained before the horizontal force in its left column exceeded a shear force calculated with the measured web section area and shear yield strength, $\sigma_y/\sqrt{3}$, are shown in this figure. Additionally, Fig. 6 and Fig. 7 show cracks in the RC walls observed at story drifts (θ) of +0.5% and +2.0%, and the measured shear distortion angle of wall segments in specimen LF-MS, respectively.

Behavior of the specimens with RC walls in the initial excursion to the first peak ($\Theta : 0\% \rightarrow +0.5\%$) distinctively differed from the behavior afterwards. In this initial excursion, strength increased roughly in a linear manner until Θ exceeded 0.3%. Strain in the steel rods increased in proportional manner with the strength of the B-B walls. Also, large initial stiffness was obtained as listed in Table 1, e.g. the measured initial stiffness for LF-M and LF-MS was 4.8 and 6.2 times as large as the stiffness of the pure frame, respectively. However, shear cracks, as shown in Fig. 6a, occurred at +0.5% drift, and strength of the B-B walls ceased to increase at this drift level; the maximum shear strength of the B-B walls was approximately 200 kN. The tension induced in the steel rods also reached the maximum at this drift level. The compressive force induced in the specimens as the reaction for the rods' tension, at this drift, was 7.4 to 9.4% of the compressive strength of the B-B wall, which is calculated using the wall's section area and the concrete's strength.

In the loading cycles following the initial excursion, both the strength of the B-B walls and tension in the steel rods decreased rapidly. Also, the maximum B-B wall's strength in negative loading, obtained at $\Theta = -0.5\%$, was smaller than the strength achieved at $\Theta = +0.5\%$. As for the damages, the concrete in the vicinity of the upper beam's lower flange initiated to spall at $\Theta = +1.0\%$. Then, towards the end of the loading ($\Theta = 2.0\%$), all the concrete of this portion fell off, leaving only the reinforcing bars to bend cyclically as loading proceeded. In all the specimens, damage of the wall concrete was severe in the upper portion of the B-B walls. In the walls of MS series specimens, shear deformation was evenly distributed in each portion (I through III) of the RC wall at $\Theta = +0.5\%$, but the deformation concentrated in the B-B wall at larger drift levels, as indicated in Fig. 7.

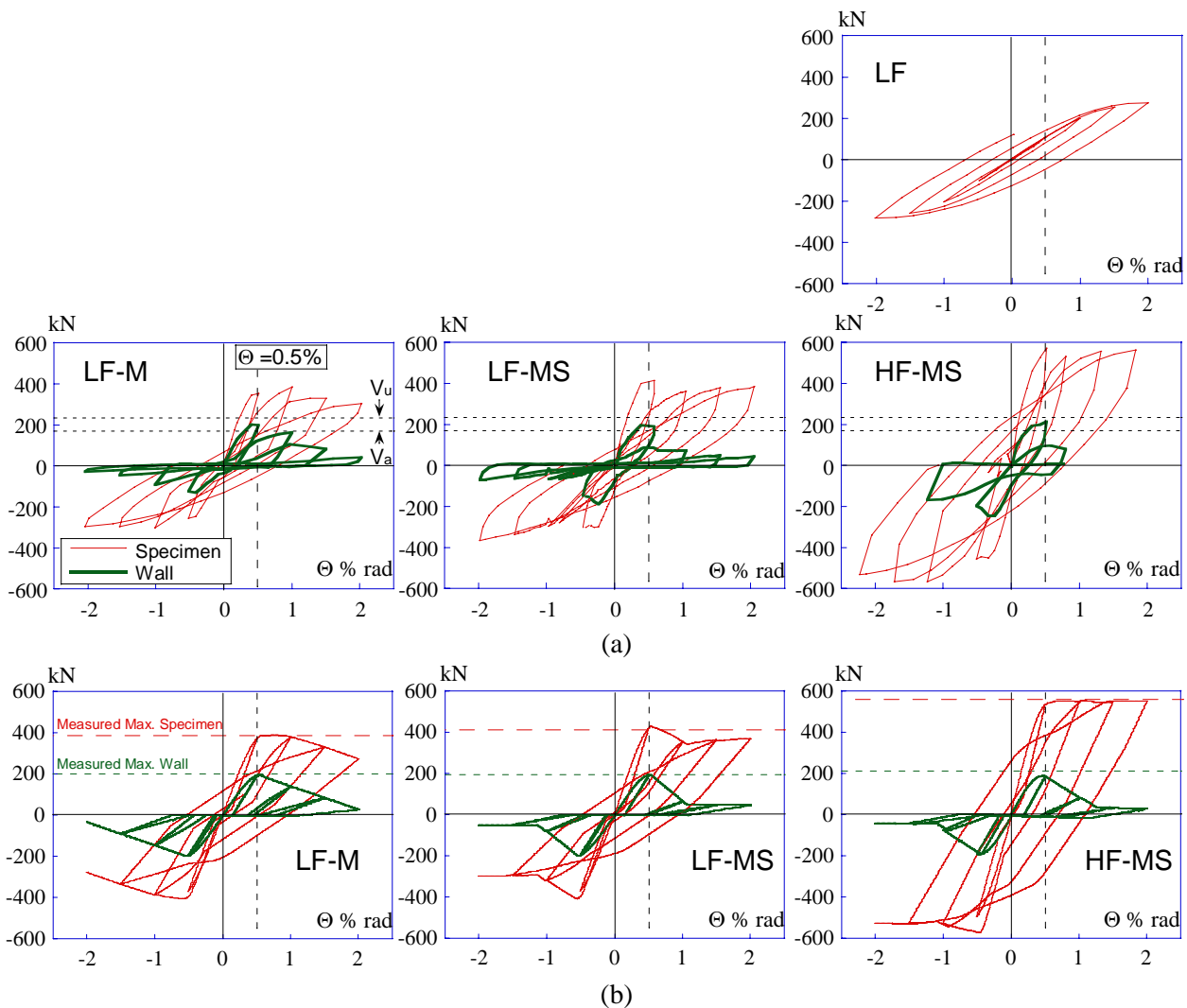


Fig. 5 Hysteresis loops: (a) test results; (b) analytical results.

The bending moment distributions in the beams also showed different patterns at 0.5% and 2.0% story drifts, as shown in Fig 8. At $\theta = +2.0\%$, bending moment was linearly distributed along the beam axis, similar to the bending moment distribution associated with the pure frame, because the B-B walls had mostly lost strength by this drift level. In contrast, the moment distribution at $\theta = +0.5\%$ shows a different pattern due to the vertical forces transferred from the B-B walls and the steel rods.

In contrast to the brittle behavior of B-B walls, the C-B wall apparently behaved in a more stable manner, based on the observation of cracks. As shown in Fig. 6a, some cracks occurred also in the C-B walls at +0.5% drift, but the crack width was not as large as those observed in B-B wall. Furthermore, concrete did not spall to the end of the tests in the C-B walls unlike the B-B walls. The bending moment distribution data also indicates stable behavior of the C-B walls. Fig 8b shows the bending moment distribution in the left side column of the MS series specimen at +0.5% and +2.0% drifts. In positive loading, the left side column connected to the C-B wall pushes the wall. In Fig 8b, one notices that, the bending moment distribution does not change linearly along the member axis, both at +0.5% and +2.0% drifts, which implies stable force transfer between the column and the C-B wall to large drift levels. In Specimen HF-MS, these forces even caused shear yielding of the left side column; this column would have plastified for bending in its upper and lower ends without the forces from the C-B walls. On the other hand, at the negative loading peaks, where the C-B wall pulls the column, the bending moment is distributed linearly along the member axis from small drift levels. To summarize, the C-B walls react with large compressive force to large drifts, but tensile reaction forces are very small from small drift levels.

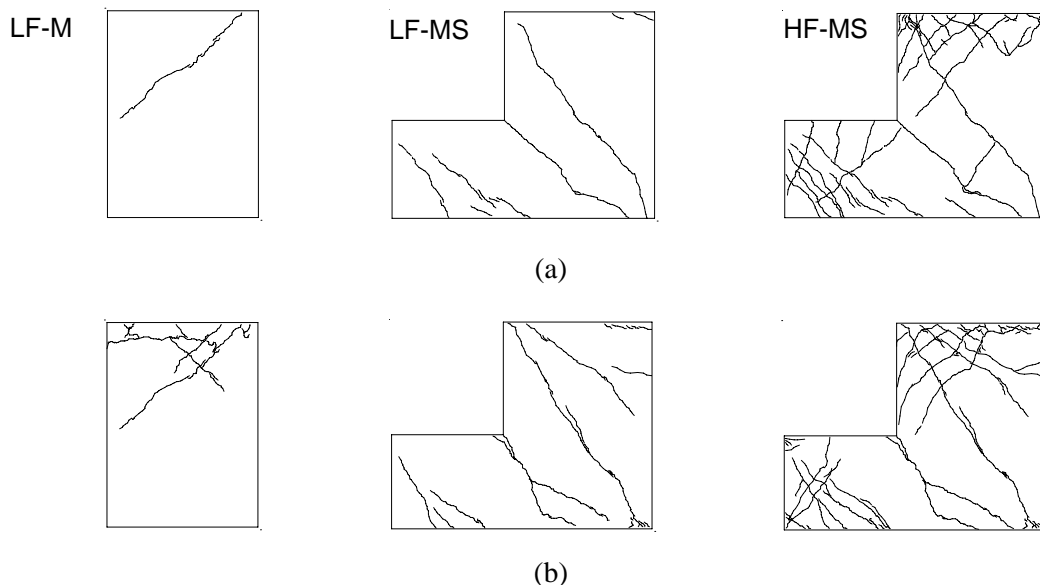


Fig. 6 Observed cracks in RC walls of specimens; (a) at 0.5% drift; (b) at 2.0% drift.

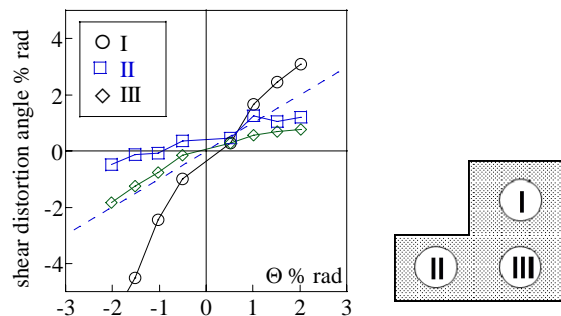


Fig. 7 RC walls' shear distortion angle v.s story drift angle relations of specimen LF-MS.

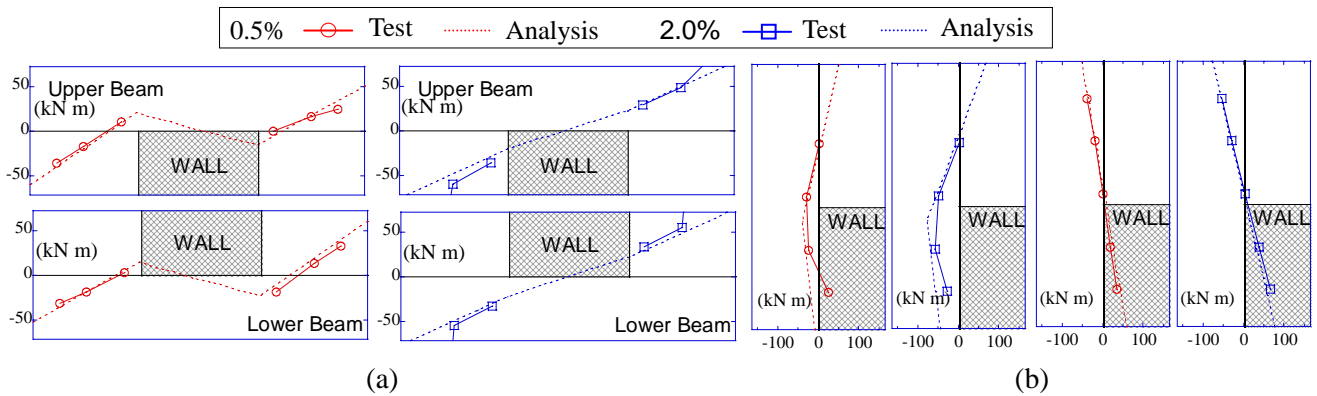


Fig. 8 Bending moment distribution obtained from tests and analyses: (a) in the beams of specimen LF-M; (b) in the left column of specimen LF-MS.

3.2 Models and verification through frame analyses

Models representing base and B-B walls are proposed based on findings by Sugiyama and Matsuzaki (2002), Ohkubo (1987) and the observation in the presented tests. The models are concrete trusses with the same material properties as those of the concrete of the tested RC walls; geometries and sections of the trusses are as follows: one end of the truss for a C-B wall is at a point on column axis, lower from the top of the C-B wall by $D_c/3$ (D_c : depth of the column); the truss extends from this point toward the lower beam at an angle of 45 degree. B-B walls are represented by one pair of trusses extending diagonally between points on the upper and lower beams at the side end of the walls (see Fig. 9a). The dimensions of the truss's section is the thickness of the wall times D_c for C-B walls, whereas for B-B walls, the section area is the thickness of the wall times $0.236 \times$ wall width, the latter being a calibrated value.

The constitutive rule used for the trusses are schematically shown in Fig. 9b. This material model includes a model for concrete proposed by Popovics (1973) for the pre-peak strength region; for the post-peak region, strength decreases linearly with the strain. Thus this model includes four parameters, E_c : Young's modulus, σ_c : compressive strength, ε_{pc} : strain at σ_c and τE_c : decreasing slope. For the analyses included herein, the measured values mentioned in section 2 are applied for E_c and σ_c . For ε_{pc} , a value smaller than the strains used conventionally for normal concrete is applied ($\varepsilon_{pc} = 0.002$), because the confinement of the concrete will be small. A calibrated value, 1/10, was applied for τ , except for the portion I of the walls (see Fig. 7) of the MS series specimens. For this wall segment, where shear distortion will concentrate, a larger value, 1/5, was used. Note that in the applied constitutive rule, hysteresis in the positive loading sequence does not affect the behavior in the negative loading, and vice versa.

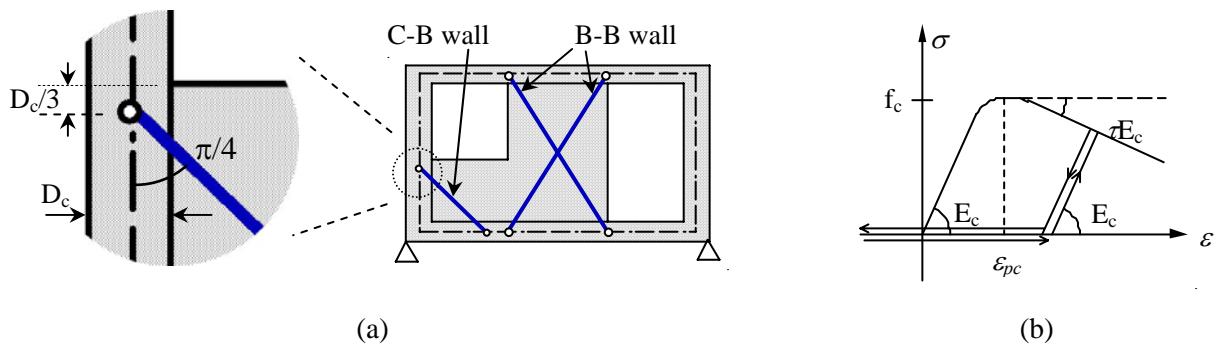


Fig. 9 Analytical model: (a) representation of wall and frame; (b) material model for truss elements.

These proposed trusses that represent the RC walls are attached to the steel frames, which are represented by fiber based line elements. The elastic perfect plastic model is used as the material model of the fibers, where the measured yield strength of the steel, shown in Table 2, is used. Beam-column elements having an axial-flexural spring and a shear spring aligned in a series, were used for columns; the strength of each springs are calculated as the flexural strength of the wide flanges under the axial load applied to the columns, and shear yielding strength of the web, respectively. Moreover, trusses that resist only in tension were applied to represent the steel rods placed at the wall's side end, although these are not shown in Fig. 9a.

The hysteresis loops obtained from 2D frame analyses using a program coded by Kawano (1998) and the proposed models are compared with the test results in Fig. 5. The analytically obtained bending moment distributions in the beam and the left column are also shown in Fig. 8. Fig. 5 shows that the models are sufficient to capture both the initial behavior and the ultimate state of the specimens; the strength obtained through analyses reach the maximum at 0.5% drift; the maximum strength is close to the test results including the results with MS series specimens. The proposed models have limitation in simulating the post-peak behavior. Nonetheless, behavior of the C-B walls, shear yielding of the left column in specimen HF-MS induced by the reaction from the C-B wall, and the strength and bending moment distribution in the frame at 2.0% drift are predicted by these simple analyses with a reasonable accuracy.

CONCLUDING REMARKS

Loading tests were conducted on three steel frame – RC wall specimens to investigate the structural behavior of B-B and C-B walls without “structural slits” to structurally isolate these elements from building frames. Behavior of these walls was linear until 0.5% drift angle, which increased stiffness of the frame to 5-6 times the stiffness of a pure frame. Strength was also increased, but shear strength of the B-B walls deteriorated rapidly beyond this drift level. Models of these walls applicable to frame analyses were created based on the test results presented in this paper and other reference. The models are sufficient to capture both the initial behavior and the ultimate state of the specimens.

REFERENCES

- AIJ. (2005). *Report on the damage investigation of the 2005 West off Fukuoka Earthquake*, AIJ.
- Kawano, A., Griffith M. C., Joshi, H.R. and Warner, R.F. (1998). Analysis of the Behavior and Collapse of Concrete Frames Subjected to Seismic Ground Motion, *Research Report No.R163*, Department of Civil and Environmental Engineering, The University of Adelaide, Australia.
- Ohkubo, M., Yamamoto, K. and Harada, T. (1987). Effect on structural performance of reinforced concrete frames by mid-span walls. *Summaries of Technical Papers of AIJ Kinki branch Annual Meeting 7*, 204-205. (in Japanese)
- Popovics, S., “A Numerical Approach to Complete Stress-Strain Curve of Concrete,” *Cement and Concrete Research*, **3**, pp.583-599, 1973.
- Sugiyama, T., Matsuzaki, Y. and Nakano, K. (2002). Structural performance of reinforced concrete frame with non-structural reinforced concrete walls. *Journal of Structural and Construction Engineering, Transactions of Architectural Institute of Japan* **551**,111-118.

ACKNOWLEDGEMENT

This research was funded by Japan Society for Promoting Science (Project Number: 17102892).